

Quasi-two-dimensional soliton in a self-repulsive spin-orbit-coupled dipolar binary condensate

S. K. Adhikari*

Instituto de Física Teórica, Universidade Estadual Paulista - UNESP, 01.140-070 São Paulo, São Paulo, Brazil

(Dated: December 23, 2025)

We study the formation of solitons in a *uniform* quasi-two-dimensional (quasi-2D) spin-orbit (SO) coupled self-repulsive binary dipolar and nondipolar Bose-Einstein condensate (BEC) using the mean-field Gross-Pitaevskii equation. For a weak SO coupling, in a nondipolar BEC, one can have three types of degenerate solitons: a multi-ring soliton with intrinsic vorticity of angular momentum projection $+1$ or -1 in one component and 0 in the other, a circularly-asymmetric soliton and a stripe soliton with stripes in the density. For an intermediate SO couplings, the multi-ring soliton ceases to exist and there appears a square-lattice soliton with a spatially-periodic pattern in density on a square lattice, in addition to the degenerate circularly-asymmetric and stripe solitons. In the presence of a dipolar interaction, with the polarization direction aligned in the quasi-2D plane, only the degenerate circularly-asymmetric and stripe solitons appear.

I. INTRODUCTION

In mathematics and physics, a soliton is a nonlinear, one-dimensional (1D) self-reinforcing, localized wave packet that is strongly stable due to a balanced cancellation of attractive nonlinear and repulsive dispersive effects in the medium. A soliton can be found in diverse systems, for example, in a water wave, in a nonlinear medium [1], in nonlinear optics [2] and in a Bose-Einstein condensate (BEC) [3]. Of these, a soliton in a BEC is especially interesting as it is a quantum system. In a quasi-1D set up, solitons have been created and studied in a BEC of ${}^7\text{Li}$ [4, 5] and ${}^{85}\text{Rb}$ [6] atoms, following the suggestion of a theoretical investigation [7], using the mean-field Gross-Pitaevskii (GP) equation [8, 9]. There are numerous examples of similar quasi-1D solitons in BECs [10–17]. Solitons have also been studied in binary BEC mixtures [18, 19]. However, stable solitons cannot be formed in two (2D) [20] and three dimensions (3D) [2, 3] due to a collapse instability.

Soon after the observation [21] of a BEC of ${}^{87}\text{Rb}$ [24], ${}^7\text{Li}$ [25] and ${}^{23}\text{Na}$ [26] atoms in a laboratory, it was possible to observe and study a hyperfine spin-one multi-component spinor BEC of ${}^{23}\text{Na}$ atoms [22]. Although it is not possible to have a natural spin-orbit (SO) coupling in electrically neutral BEC atoms, an artificial synthetic SO coupling can be created by tuning a pair of Raman lasers beams which couple the different hyperfine spin states [23, 27, 28]. Dresselhaus [29] and Rashba [30] suggested two possible ways of creating such SO couplings. An equal mixture of Dresselhaus and Rashba SO couplings has been experimentally realized in a BEC of ${}^{87}\text{Rb}$ [31] and ${}^{23}\text{Na}$ [32] atoms of $F_z = 0, -1$ hyperfine components. The mean-field binary GP equation of such an SO-coupled BEC is coupled by the Pauli spin matrices and hence this BEC is called a pseudo spin-half BEC.

Multi-component spinor BECs possess distinct properties and can have different excitations [33, 34], which are not allowed in a single-component scalar BEC. For example, a quasi-1D [35], a quasi-2D [36, 37] or a 3D [38] soliton can be stabilized in an SO-coupled binary BEC, which can have distinct spatial structure. Later, SO-coupled BECs were studied [27] and an SO-coupled spin-one condensate of ${}^{87}\text{Rb}$ atoms in hyperfine states $F_z = \pm 1, 0$ was investigated [39]. A spin-one SO-coupled multi-component BEC also sustains a quasi-1D [40] or a quasi-2D [41] or a 3D [42] soliton, not possible in a single-component BEC [20].

The studies of quasi-2D [41] and 3D [42] solitons in an SO-coupled nondipolar binary BEC indicate that the SO coupling introduces a stabilizing attractive interaction necessary for the formation of a self-bound soliton. All previous studies on SO-coupled nondipolar BEC solitons were performed on a self-attractive system with a negative atomic scattering length [36, 37, 41] corresponding to an attraction among the atoms, which facilitates the formation of a soliton. A positive atomic scattering length corresponds to a repulsion among the atoms [21]. However, the scattering length in a BEC can often be varied continuously from positive to negative, thus turning the system attractive from repulsive, by changing an external background magnetic field near a Feshbach resonance [43, 44]. In fact, this technique was used to change the scattering length of ${}^{85}\text{Rb}$ atoms in the BEC from a positive value (repulsive interaction) to a negative value (attractive interaction) to facilitate the formation of a soliton. In this fashion a self-attractive BEC of ${}^{85}\text{Rb}$ atoms was obtained and a quasi-1D soliton was created and studied [6] in this system in a laboratory. In a different front it was demonstrated [45] that it is possible to have a stable anisotropic soliton in a quasi-2D dipolar BEC with the polarization direction lying in the quasi-2D plane. There have also been many studies of quasi-1D solitons in dipolar BECs under different conditions [46–49].

The long-range nonlocal anisotropic dipolar interaction sets up a different scenario [45] for the stabilization of a

*sk.adhikari@unesp.br

<https://professores.ift.unesp.br/sk.adhikari/>

quasi-2D soliton, which will not be possible in the absence of a dipolar interaction [20]. Many new phenomena are possible in a dipolar BEC, such as, angular collapse [50], roton mode [51, 52], quasi-2D asymmetric soliton [45], quantum droplet [53], supersolidity in 1D [54] and 2D [55], anisotropic expansion [56] etc. The study of a dipolar BEC got new impetus after the experimental observation of dipolar BECs of ^{52}Cr [57–59], ^{166}Er [60], ^{168}Er [61], and ^{164}Dy [62, 63] atoms, with large magnetic dipole moment. In contrast to previous studies [36, 37, 64, 65] of SO-coupled binary quasi-2D solitons in a self-attractive BEC, here we perform a comprehensive study of quasi-2D solitons in a binary Rashba or a Dresselhaus SO-coupled self-repulsive nondipolar and also dipolar BEC with positive scattering lengths, where the polarization direction of the dipolar atoms lies in the quasi-2D plane. The solitons in this system are bound due to a joint action of the SO coupling and the long-range dipolar interaction, in spite of the short-range contact repulsion in a self-repulsive binary BEC and new types of 2D solitons are expected in this system. We find drastic changes in soliton structure and density in an SO-coupled binary BEC soliton after the introduction of a weak dipolar interaction. There have been a few previous studies on different aspects of an SO-coupled dipolar BEC [28, 66–71].

We find different types solitons in an SO-coupled quasi-2D binary nondipolar self-repulsive BEC. For a small value of SO-coupling strength parameter γ ($0 < \gamma \lesssim 1$) there can be three types of degenerate solitons. The first type is a $(\mp 1, 0)$ -type multi-ring soliton, where the numbers in the parenthesis represent the angular momentum projections of the two components with the upper (lower) sign corresponding to Rashba (Dresselhaus) SO coupling. This state has $1/2$ unit of angular momentum projection and is often called a half-quantum vortex state [72]. This half-quantum vortex state has been experimentally observed and studied in a topological superfluid ^3He [73]. The second type is a stripe soliton with a spatially-periodic stripe pattern in density of the two components and no such stripe in the total density. Such stripe pattern in a pseudo spin-half SO-coupled BEC of ^{23}Na atoms was experimentally observed [32]. The third type is a circularly-asymmetric soliton. The component densities and total density of a circularly-asymmetric soliton are also circularly-asymmetric. For medium SO coupling ($\gamma \gtrsim 1$), the aforementioned half-quantum vortex multi-ring soliton ceases to exist and we find three different types of degenerate solitons in a nondipolar binary BEC, e.g., a stripe soliton, a circularly-asymmetric soliton, and a square-lattice soliton with a spatially periodic 2D structure along both x and y directions.

The aforementioned spatially-periodic stripe [74–78] and square-lattice [65] pattern in an SO-coupled BEC is intimately related to a similar pattern in a supersolid [79–83]. A supersolid is a special quantum state of matter with a rigid spatially-periodic crystalline structure [84], breaking continuous translational invariance, that flows with zero viscosity as a superfluid breaking continuous

gauge invariance.

The introduction of a dipolar interaction in an SO-coupled BEC changes the scenario of soliton formation [45]. The dipolar interaction with the polarization direction in the quasi-2D x - y plane breaks the circular symmetry in this plane. Consequently, the quasi-2D soliton gets stretched along the polarization direction. Because of this stretching, the square-lattice soliton ceases to exist and in this case we have only two types of degenerate solitons in a quasi-2D self-attractive or self-repulsive SO-coupled dipolar binary BEC: stripe solitons and circularly-asymmetric solitons. For all cases studied in this paper, the density and energy of the solitons are the same for Rashba and Dresselhaus SO couplings, although the two wave functions are different. In the presence of an SO coupling, magnetization is not conserved; However, the magnetization of most solitons studied in this paper is zero.

In Sec. II A we present the mean-field GP equation for the SO-coupled BEC in dimensionless form appropriate for the study of a quasi-2D soliton. In Sec. II B we present an analytic study of the eigenfunctions of the quasi-2D solitons and identify the origin of the degenerate multi-ring, stripe, and square-lattice solitons. In Sec. III we present the numerical results of this investigation. In the nondipolar SO-coupled self-repulsive and self-attractive quasi-2D BEC we identify four types of solitons as elaborated in Sec. III A: the multi-ring, stripe, circularly-asymmetric, and square-lattice solitons. However, in the dipolar self-repulsive and self-attractive cases we find only two types of solitons as presented in Sec. III B: the stripe and circularly-asymmetric solitons. Finally, in Sec. IV we present a brief summary of this investigation.

II. MEAN-FIELD MODEL

A. Gross-Pitaevskii equation

We consider a binary SO-coupled BEC of N atoms, two components $j = 1, 2$, each of mass m , under a harmonic trap $V(\mathbf{r}) = m\omega_\rho^2(x^2 + y^2)/2 + m\omega_z^2 z^2/2$ ($\omega_z \gg \omega_\rho$) of frequency ω_z along the z axis and ω_ρ in the quasi-2D x - y plane. The single particle Hamiltonian of the SO-coupled BEC is [31]

$$H_0 = -\frac{\hbar^2}{2m}(\partial_x^2 + \partial_y^2 + \partial_z^2) + V(\mathbf{r}) + \gamma[\eta p_y \sigma_x - p_x \sigma_y], \quad (1)$$

where $\mathbf{r} \equiv \{x, y, z\}$, $\boldsymbol{\rho} \equiv \{x, y\}$, $\partial_x = \partial/\partial x$ etc., γ is the strength of the SO-coupling interaction, for Rashba (Dresselhaus) coupling the parameter $\eta = +1$ ($\eta = -1$), $p_x = -i\hbar\partial_x$ and $p_y = -i\hbar\partial_y$, with $i = \sqrt{-1}$, are the momentum along x and y axes, respectively, and the

Pauli spin matrices σ_x and σ_y are

$$\sigma_x = \begin{pmatrix} 0 & 1 \\ 1 & 0 \end{pmatrix}, \quad \sigma_y = \begin{pmatrix} 0 & -i \\ i & 0 \end{pmatrix}. \quad (2)$$

The intraspecies ($V_j, j = 1, 2$) and interspecies (V_{12}) interactions for two atoms at positions \mathbf{r} and \mathbf{r}' are given by [57]

$$V_j(\mathbf{R}) = \frac{\mu_0\mu^2}{4\pi}V_{\text{dd}}(\mathbf{R}) + \frac{4\pi\hbar^2a_j}{m}\delta(\mathbf{R}), \quad (3)$$

$$V_{12}(\mathbf{R}) = \frac{\mu_0\mu^2}{4\pi}V_{\text{dd}}(\mathbf{R}) + \frac{4\pi\hbar^2a_{12}}{m}\delta(\mathbf{R}), \quad (4)$$

$$V_{\text{dd}}(\mathbf{R}) = \frac{1 - 3\cos^2\theta}{\mathbf{R}^3}, \quad (5)$$

where $\mathbf{R} \equiv (\mathbf{r} - \mathbf{r}')$ is the position vector joining the two atoms, μ_0 is the permeability of free space, μ is the magnetic dipole moment of each atom, θ is the angle made by the vector \mathbf{R} with the polarization y direction, a_j is the intraspecies scattering length, and a_{12} is the interspecies scattering length. To compare the dipolar and contact interactions, the dipolar interaction is expressed in terms of the dipolar length, defined by [57]

$$a_{\text{dd}} \equiv \frac{\mu_0\mu^2m}{12\pi\hbar^2}. \quad (6)$$

In the actual experimental realization of an SO-coupled binary dipolar BEC of equal-mass atoms we can consider a binary ^{164}Dy - ^{162}Dy BEC. The atomic masses of these two isotopes of the dysprosium atom are almost equal, which justifies the equal mass approximation. The magnetic dipole moment of each species is $\mu = 10\mu_B$, where μ_B is a Bohr magneton. Hence the two species of atoms have the same dipole moment, same intraspecies and interspecies dipolar interactions and the dipolar lengths of the two components are equal. As the nuclear spin of both atoms – ^{164}Dy and ^{162}Dy – is zero, there is no hyperfine structure. Nevertheless, a synthetic SO coupling can be established in this binary system involving different types of atoms, particularly in the context of ultracold atomic gases used for quantum simulation. Dipolar BECs of both ^{164}Dy [62, 85] and ^{162}Dy [86, 87] atoms have been experimentally realized [88] and are now routinely studied in different laboratories. The interspecies and intraspecies scattering lengths of this binary dipolar BEC are all positive [88, 89], corresponding to a self-repulsion among the ingredients, which will make the formation of a soliton difficult.

In the case of a nondipolar SO-coupled binary mixture we consider two hyperfine spin states, $F_z = 0, -1$, of the ^{87}Rb atom with positive scattering lengths [90]. Such an SO-coupled mixture has already been observed [31] and studied in a laboratory [91]. This binary BEC seems to be an ideal system for the study of a self-repulsive SO-coupled binary mixture with equal atomic masses.

This dipolar binary BEC of two components $j = 1, 2$

is described by the following set of equations [57, 92]

$$\begin{aligned} i\hbar\partial_t\phi_j(\mathbf{r}, t) = & \frac{\hbar^2}{m} \left[-\frac{1}{2}(\partial_x^2 + \partial_y^2 + \partial_z^2) + \frac{m^2}{2\hbar^2}(\omega_\rho^2\rho^2 + \omega_z^2z^2) \right. \\ & + 4\pi ma_j N_j |\phi_j(\mathbf{r}, t)|^2 + 4\pi a_{12} N_k |\phi_k(\mathbf{r}, t)|^2 \\ & + 3a_{\text{dd}} N_j \int V_{\text{dd}}(\mathbf{R}) |\phi_j(\mathbf{r}', t)|^2 d\mathbf{r}' \\ & \left. + 3a_{\text{dd}} N_k \int V_{\text{dd}}(\mathbf{R}) |\phi_k(\mathbf{r}', t)|^2 d\mathbf{r}' \right] \phi_j(\mathbf{r}, t), \\ & j \neq k = 1, 2, \end{aligned} \quad (7)$$

where $\partial_t \equiv \partial/\partial t$, N_j and N_k are the number of atoms in the two components ($N = N_1 + N_2$). The dipolar atoms are polarized along the x direction. Equations (7) can be cast in the following dimensionless form if we scale lengths in units of $l_0 = \sqrt{\hbar/m\omega_z}$, time units of $t_0 = 1/\omega_z$, density in units of l_0^{-2} , and energy in units of $\hbar\omega_z$

$$\begin{aligned} i\partial_t\phi_j(\mathbf{r}, t) = & \left[-\frac{1}{2}(\partial_x^2 + \partial_y^2 + \partial_z^2) + \frac{1}{2} \left(\frac{\omega_\rho^2}{\omega_z^2}\rho^2 + z^2 \right) \right. \\ & + 4\pi a_j N_j |\phi_j(\mathbf{r}, t)|^2 + 4\pi a_{12} N_k |\phi_k(\mathbf{r}, t)|^2 \\ & + 3a_{\text{dd}} N_j \int V_{\text{dd}}(\mathbf{R}) |\phi_j(\mathbf{r}', t)|^2 d\mathbf{r}' \\ & \left. + 3a_{\text{dd}} N_k \int V_{\text{dd}}(\mathbf{R}) |\phi_k(\mathbf{r}', t)|^2 d\mathbf{r}' \right] \phi_j(\mathbf{r}, t), \end{aligned} \quad (8)$$

where $j \neq k = 1, 2$. Without any risk of confusion, here and in the following we are using the same symbols to denote the scaled dimensionless and unscaled variables.

We consider a quasi-2D binary dipolar BEC with a strong trap along the z direction. We assume that the dynamics of the BEC in the z direction is confined in the ground state

$$\psi_B(z) = \pi^{-1/4} e^{-z^2/2}. \quad (9)$$

The component wave function of the BEC can be written as

$$\phi_j(\mathbf{r}, t) = \psi_B(z) \times \psi_j(\boldsymbol{\rho}, t), \quad (10)$$

where $\psi_i(\boldsymbol{\rho}, t)$ is the wave function of the quasi-2D BEC confined in the x - y plane. The relevant dynamics in the x - y plane, obtained by integrating out the z coordinate [93], leads to the following set of GP equations for the two components [92, 94]

$$\begin{aligned} i\partial_t\psi_j(\boldsymbol{\rho}, t) = & \left[-\frac{1}{2}(\partial_x^2 + \partial_y^2) + c_1 n_j(\boldsymbol{\rho}, t) + c_2 n_k(\boldsymbol{\rho}, t) \right. \\ & \left. + d \sum_{j=1,2} s_j(\boldsymbol{\rho}, t) \right] \psi_j(\boldsymbol{\rho}, t) - \gamma[i\eta\partial_y \\ & + (-1)^j \partial_x] \psi_k(\boldsymbol{\rho}, t), \quad j \neq k = 1, 2, \end{aligned} \quad (11)$$

$$s_j(\boldsymbol{\rho}, t) = \int \frac{d\mathbf{k}_\rho}{(2\pi)^2} e^{-i\mathbf{k}_\rho \cdot \boldsymbol{\rho}} \tilde{n}_j(\mathbf{k}_\rho, t) j_{2D} \left(\frac{k_\rho}{\sqrt{2}} \right), \quad (12)$$

$$j_{2D}(\xi) = \frac{1}{2\pi} \int_{-\infty}^{\infty} dk_z \left(\frac{3k_y^2}{k^2} - 1 \right) |\tilde{n}(k_z)|^2, \\ = \frac{1}{\sqrt{2\pi}} \left[-1 + 3\sqrt{\pi} \frac{\xi^2}{\xi} e^{\xi^2} \{1 - \text{erf}(\xi)\} \right], \quad (13)$$

$$\xi = \frac{k_\rho}{\sqrt{2}}, \quad \xi_y = \frac{k_y}{\sqrt{2}}, \quad k_\rho = \sqrt{k_x^2 + k_y^2}, \quad (14)$$

$$\tilde{n}_j(\mathbf{k}_\rho, t) = \int d\rho e^{i\mathbf{k}_\rho \cdot \rho} |\psi_j(\rho, t)|^2, \quad (15)$$

$$\tilde{n}(k_z) = \int_{-\infty}^{\infty} dk_z e^{ik_z z} |\psi_B(z)|^2 = e^{-k_z^2/4^2}, \quad (16)$$

where $d = 4\pi a_{\text{dd}} N$, $c_1 = 2N\sqrt{2\pi}a$, $c_2 = 2N\sqrt{2\pi}a_{12}$ and we have included the SO-coupling terms and assumed that $a_1 = a_2 \equiv a$. Here $n_j(\rho, t) = |\psi_j(\rho, t)|^2$, $j = 1, 2$ are the densities of the two components, and $n(\rho, t) = \sum_j n_j(\rho, t)$ the total density. In this study of quasi-2D solitons in the x - y plane we have dropped the harmonic oscillator trapping potential from Eqs. (11). The normalization condition is $\int n(\rho) d\rho = 1$.

The time-independent version of Eqs. (11), appropriate for stationary solutions, can be derived from the energy functional

$$E[\psi_j] = \frac{1}{2} \int_{-\infty}^{\infty} dx \int_{-\infty}^{\infty} dy \left[\sum_{j=1}^2 (|\partial_x \psi_j|^2 + |\partial_y \psi_j|^2) \right. \\ \left. + c_1(n_1^2 + n_2^2) + 2c_2 n_1 n_2 + d(s_1^2 + s_2^2) + 2ds_1 s_2 \right. \\ \left. + 2\gamma \{ \psi_1^* (\partial_x - i\eta \partial_y) \psi_2 - \psi_2^* (\partial_x + i\eta \partial_y) \psi_1 \} \right]. \quad (17)$$

B. Analytic Consideration

Many properties of a binary nondipolar or dipolar, self-repulsive or self-attractive SO-coupled uniform BEC can be understood from a consideration of the eigenfunction-eigenvalue problem of the linear Hamiltonian, setting all nondipolar and dipolar nonlinear interactions and the confining trap to zero [$c_1 = c_2 = d = V(\mathbf{r}) = 0$]. The quasi-2D stationary wave function of the linear single-particle trapless Hamiltonian corresponding to Eq. (1)

$$H_0^{2D} = -\frac{1}{2}(\partial_x^2 + \partial_y^2) - i\gamma[\eta \partial_y \sigma_x - \partial_x \sigma_y] \quad (18)$$

satisfies the following eigenfunction-eigenvalue problem

$$\begin{bmatrix} -\frac{1}{2}(\partial_x^2 + \partial_y^2) & \gamma(\partial_x - i\eta \partial_y) \\ -\gamma(\partial_x + i\eta \partial_y) & -\frac{1}{2}(\partial_x^2 + \partial_y^2) \end{bmatrix} \begin{pmatrix} \psi_1 \\ \psi_2 \end{pmatrix} = \mathcal{E} \begin{pmatrix} \psi_1 \\ \psi_2 \end{pmatrix}, \quad (19)$$

with energy eigenvalue \mathcal{E} . In circular coordinates $\rho = \{\rho, \theta\}$, $x = \rho \cos \theta$, $y = \rho \sin \theta$, and we have $(\partial_x \pm i\partial_y) = \exp(\pm i\theta)(\partial_\rho \pm i\partial_\theta/\rho)$, with $\partial_\rho \equiv \partial/\partial\rho$, $\partial_\theta \equiv \partial/\partial\theta$. A circularly-symmetric solution of angular momentum projection m of Eq. (19) has the form [72]

$$\begin{pmatrix} \psi_1(\rho) \\ \psi_2(\rho) \end{pmatrix} = \begin{pmatrix} \psi_1(\rho) \\ \psi_2(\rho) \exp(i\eta\theta) \end{pmatrix} \frac{\exp(im\theta)}{\sqrt{2\pi}}, \quad (20)$$

with two equivalent ground states. For the first state, $m = 0$ and the second component has a phase $\exp(i\eta\theta)$ relative to the first component. This state is of type $(0, \eta)$ or $(0, \pm 1)$ for Rashba (upper sign) or Dresselhaus (lower sign) SO coupling. The second state has $m = -\eta$ with the first component carrying a phase $\exp(-i\eta\theta)$ relative to the second component. This state is of type $(-\eta, 0)$ or $(\mp 1, 0)$ for Rashba or Dresselhaus SO coupling. Of these two types of equivalent states, in this study we consider only the state of type $(\mp 1, 0)$. These states have angular momentum projection $m = 0$ and spin $s = 1/2$, hence the total angular momentum projection $j_z = m + s_z = \pm 1/2$ and these states are often called half-quantum vortex states. However, if we consider larger values of $|m| > 1$ in Eq. (20), we can have excited states of type $(\mp 2, \mp 1)$, $(\mp 3, \mp 2)$ etc. of larger energy. In an actual nondipolar SO-coupled uniform BEC for small γ the infinite ground state of type $(\mp 1, 0)$ becomes a localized multi-ring soliton.

Equation (19) also has the following four degenerate solutions

$$\begin{pmatrix} \psi_1 \\ \psi_2 \end{pmatrix} = \begin{pmatrix} \cos(\gamma x) \\ -\sin(\gamma x) \end{pmatrix}, \quad \begin{pmatrix} \psi_1 \\ \psi_2 \end{pmatrix} = \begin{pmatrix} \sin(\gamma x) \\ \cos(\gamma x) \end{pmatrix}, \quad (21)$$

$$\begin{pmatrix} \psi_1 \\ \psi_2 \end{pmatrix} = \begin{pmatrix} \cos(\gamma y) \\ -i\eta \sin(\gamma y) \end{pmatrix}, \quad \begin{pmatrix} \psi_1 \\ \psi_2 \end{pmatrix} = \begin{pmatrix} \sin(\gamma y) \\ i\eta \cos(\gamma y) \end{pmatrix}, \quad (22)$$

with energy eigenvalue

$$\mathcal{E} = -\frac{\gamma^2}{2}. \quad (23)$$

The solutions (21) and (22) represent stripes along x and y directions, respectively, with a spatial period of π/γ in density. Both sets of solutions have uniform density in the sum of the two components: $|\psi_1|^2 + |\psi_2|^2 = 1$. The energy and the density of the states are the same for both Rashba and Dresselhaus SO couplings. In an actual nondipolar or dipolar self-attractive and self-repulsive SO-coupled uniform BEC the infinite ground state with stripe becomes a localized stripe soliton with the same density and energy for both Rashba and Dresselhaus SO couplings.

A linear combination of the degenerate states (21) and (22), e.g.

$$\begin{pmatrix} \psi_1 \\ \psi_2 \end{pmatrix} = \sqrt{n} \begin{pmatrix} \cos(\gamma x) \pm \cos(\gamma y) \\ -\sin(\gamma x) \mp i\eta \sin(\gamma y) \end{pmatrix}, \quad (24)$$

is also a valid degenerate eigenfunction of Eq. (19) with energy $\mathcal{E} = -\gamma^2/2$ and represents an infinite square-lattice pattern in density of the components as well as in the total density. In an actual nondipolar self-attractive and self-repulsive SO-coupled uniform BEC, for medium values of γ , the infinite square-lattice ground state becomes a localized square-lattice soliton with the same density and energy for both Rashba and Dresselhaus SO couplings.

Equations (20), (21) and (22), and (24) describe three possible infinite eigenstates of a uniform binary SO-coupled linear system governed by the Hamiltonian (18).

We will see in the following that, the eigenstates for the localized binary SO-coupled solitons, controlled by Eq. (11), may be well approximated by the eigenstates (20), (21) and (22), and (24) times an appropriate Gaussian function, which gives the localization of the soliton. Hence in the numerical calculation employing imaginary-time propagation of the wave function of the localized binary SO-coupled nondipolar and dipolar solitons, we will be using these approximations as the initial states.

III. NUMERICAL RESULT

To solve the binary equations (11) numerically, we propagate these in time by the split-time-step Crank-Nicolson discretization scheme [95]. As we require to solve the GP equation in presence of both SO-coupling and dipolar interaction, we needed to combine the Open Multiprocessing Programs for solving the dipolar [94, 96] and SO-coupled [97] GP equations. We employ space steps of $dx = dy = 0.1$ and a time step of $dt = dx \times dy \times 0.1$ for imaginary-time propagation. In all calculations of stationary states, we employ imaginary-time approach with the conservation of total normalization

$$\int_{-\infty}^{\infty} dx \int_{-\infty}^{\infty} dy [n_1(x, y) + n_2(x, y)] = 1 \quad (25)$$

during time propagation, which finds the lowest-energy solution of each type. The magnetization

$$M = \frac{\int_{-\infty}^{\infty} dx \int_{-\infty}^{\infty} dy [n_1(x, y) - n_2(x, y)]}{\int_{-\infty}^{\infty} dx \int_{-\infty}^{\infty} dy [n_1(x, y) + n_2(x, y)]}, \quad (26)$$

is not a good quantum number in the presence of spin-mixing SO coupling and is left to freely evolve during time propagation to attain a final converged value consistent with the parameters of the problem. In the presence of SO coupling the number of atoms in each component is not conserved. The converged value of the magnetization M was found to be negligibly small in most cases for values of γ considered in this paper indicating an almost equal number of atoms in the two components. For $\gamma = 0$, the magnetization is strictly equal to zero.

We find different types of soliton with different spatial symmetry properties in our numerical investigation by imaginary-time propagation. In order to obtain the stripe soliton, we use the stripe function (21) times a Gaussian function as the initial state in imaginary-time propagation. To obtain the square-lattice soliton in imaginary-time propagation in an efficient way, we use the function (24) multiplied by a Gaussian function as the initial state. To obtain the circularly-asymmetric soliton, we use localized Gaussian functions as the initial state in imaginary-time propagation. Finally, to obtain a multi-ring ($\mp 1, 0$) soliton, we print the vortex structure, viz. Eq. (20), on the initial Gaussian function.

In an actual experiment, by carefully ramping up the intensity of the Raman beams used to create the SO coupling and adjusting the detuning, the system undergoes

a phase transition into the stripe phase. The competition between the interaction energy and the SOC term in the Hamiltonian leads to a ground state where the atoms condense in a superposition of two finite-momentum states, spontaneously breaking the translational symmetry of space. The multi-ring phase can be achieved by imprinting an appropriate vortex by a laser on the BEC.

A. Quasi-2D SO-coupled binary self-repulsive nondipolar BEC soliton

We study the formation of different types of soliton in a quasi-2D SO-coupled binary self-repulsive and self-attractive dipolar and nondipolar BEC. For a self-repulsive BEC the scattering lengths a and a_{12} are positive indicating a repulsive intra-component and inter-component interaction. Hence, in this system no solitons are possible in the absence of a dipolar interaction and SO coupling. Both a dipolar interaction [45] and an SO coupling [36] contribute to an attraction in the system and it helps to form a bound soliton. Here, we demonstrate that in the presence of SO coupling alone, the system may become attractive and allow the formation of a quasi-2D soliton.

Without losing generality we consider a nondipolar BEC with a small value of the nonlinearity parameters $c_1 = c_2 = 0.25$ in Eqs. (11), so that a soliton can be formed for a small value of the SO-coupling strength γ , which facilitates both theoretical and numerical investigations. For a small γ ($\gamma = 0.5$) we find three types of degenerate solitons in a self-repulsive nondipolar BEC. First, there is a ($\mp 1, 0$)-type multi-ring soliton for Rashba (upper sign) or Dresselhaus (lower sign) SO coupling. In Fig. 1 we display the contour plot of density of the central region of components (a) $j = 1$, (b) $j = 2$, and (c) total density of a ($\mp 1, 0$)-type multi-ring soliton. The left (middle) column shows the density of component $j = 1$ ($j = 2$), whereas the right column illustrates the total density. The density is independent of whether we employ Dresselhaus SO coupling or Rashba SO coupling. However, the phase of this ($+1, 0$)-type Dresselhaus SO-coupled soliton is distinct from a ($-1, 0$)-type Rashba SO-coupled soliton. In Figs. 2(a)-(b) we display the contour plot of the phase of wave function components $j = 1, 2$ of the ($+1, 0$)-type Dresselhaus SO-coupled soliton of Figs. 1(a)-(c). In Fig. 2(a) there is a phase drop of $+2\pi$ under a complete rotation, indicating an angular momentum projection of $+1$ (vortex of unit angular momentum) in component $j = 1$ and 0 in component $j = 2$. The corresponding phases for Rashba SO coupling are illustrated in Figs. 2(c)-(d) showing the phases of the wave-function components $j = 1, 2$ of the SO-coupled soliton. In this case in Fig. 2(c) we find a phase drop of -2π under a complete rotation around the origin, indicating an angular momentum projection of -1 (anti-vortex of unit angular momentum) in component $j = 1$ and 0 in component $j = 2$, viz. Fig. 2(d). In addition to

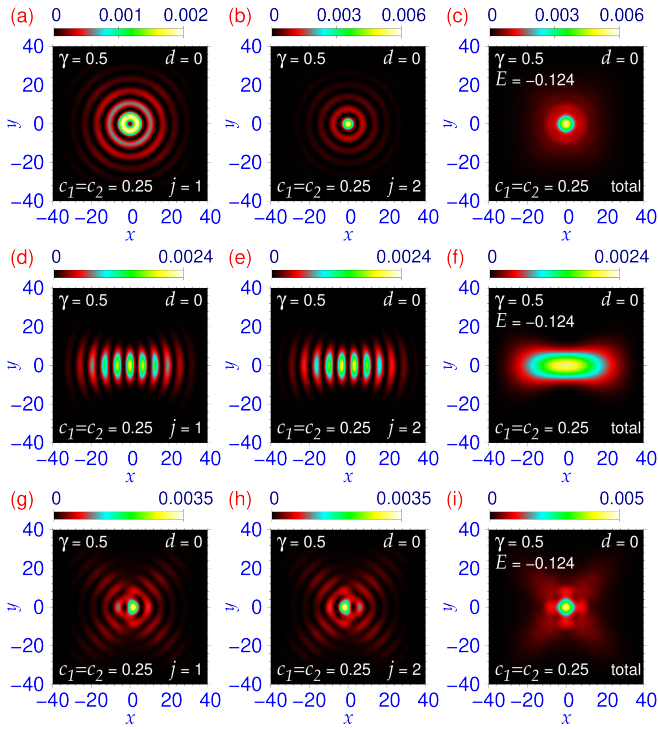


FIG. 1: Contour plot of density n_j of a quasi-2D nondipolar ($\mp 1, 0$)-type binary Rashba or Dresselhaus SO-coupled BEC soliton for components (a) $j = 1$ (n_1), (b) $j = 2$ (n_2) and (c) total density (n); the same of a stripe soliton for components (d) $j = 1$, (e) $j = 2$ and (f) total density; and of a circularly-asymmetric soliton for (g) $j = 1$, (h) $j = 2$ and (i) total density. In this figure and in Figs. 3, 4, 5 and 6 the energy is given in the plots of total density in the last column. The parameters are $c_1 = c_2 = 0.25$, $\gamma = 0.5$. The plotted quantities in all figures of this paper are dimensionless.

the multi-ring solitons, for $\gamma = 0.5$ we can also have stripe solitons with stripes in density, of a spatial period π/γ , of both the components as shown in Figs. 1(d)-(f) for components $j = 1, 2$ and total density, respectively. However, the total density of the two components is without any stripe pattern as shown in Fig. 1(f). Moreover, we have a circularly-asymmetric soliton as shown in Figs. 1(g)-(i), where we display the density of the two components and the total density, respectively. A close examination of the soliton components $j = 1, 2$ in Figs. 1(g)-(h), respectively, reveals the presence of asymmetrically located vortex-anti-vortex pairs, explicitly demonstrated through a contour plot of the phase of these wave-function components in Figs. 2(e)-(f). The component densities are zero (black) in Figs. 1(g)-(h) at the position of vortex and anti-vortex in Figs. 2(e)-(f), but the total density is not zero at these points, indicating that these are coreless. These three types of solitons are degenerate with the numerical energy $\mathcal{E} = -0.124$ close to its theoretical estimate $\mathcal{E} = \gamma^2/2 = -0.125$ for $\gamma = 0.5$. In this case no square-lattice soliton could be found. The scenario

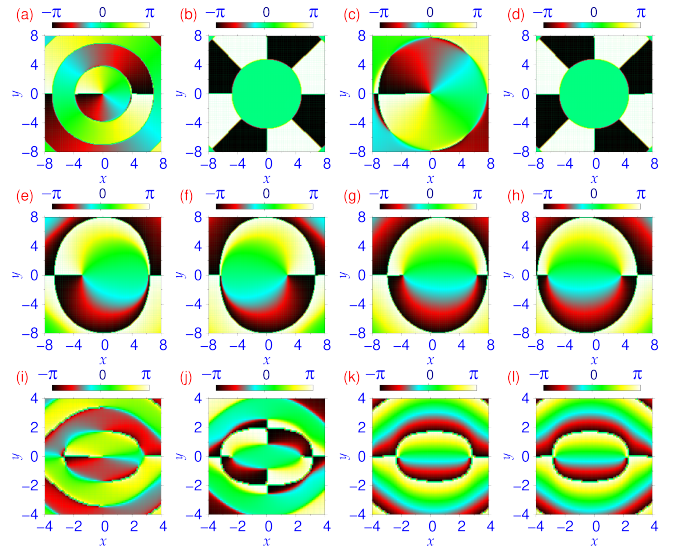


FIG. 2: Contour plot of phase of wave-function components (a) $j = 1$, and (b) $j = 2$ of the quasi-2D Dresselhaus SO-coupled multi-ring soliton of Figs. 1(a)-(b); the same of wave-function components (c) $j = 1$, and (d) $j = 2$ of a Rashba SO-coupled soliton of Figs. 1(a)-(b); of wave-function components (e) $j = 1$, and (f) $j = 2$ of the Dresselhaus SO-coupled soliton of Figs. 1(g)-(h); of wave-function components (g) $j = 1$, (h) $j = 2$ of the Dresselhaus SO-coupled dipolar soliton of Figs. 4(g)-(h); of wave-function components (i) $j = 1$, (j) $j = 2$ of the Dresselhaus SO-coupled dipolar soliton of Figs. 5(a)-(b); of wave-function components (k) $j = 1$, (l) $j = 2$ of the Dresselhaus SO-coupled dipolar soliton of Figs. 5(d)-(e).

of soliton formation does not change for a self-attractive nondipolar BEC, where there are also these three types of soliton (result not presented in this paper). The degeneracy of the states depicted in Fig. 3, for small values of nonlinearities ($c_1 = 0.25$, $c_2 = 0.25$ and $d = 0$), is a consequence of the degeneracy of the states in the linear problem in Sec. II B, viz. Eqs. 20, (21)-(24). The degeneracy will disappear for a larger value of the nonlinearities.

As γ is increased, a new scenario of soliton formation emerges. However, the types of solitons for $\gamma = 1$ to $\gamma = 3$ are quite similar and here we concentrate on $\gamma = 2$. For $\gamma = 2$, we find three types of degenerate solitons in a quasi-2D nondipolar self-repulsive SO-coupled BEC. The ($\mp 1, 0$)-type multi-ring soliton, viz. Figs. 1(a)-(c), ceases to exist and gives rise to a new type of soliton: a square-lattice soliton with square-lattice modulation in density. This soliton is illustrated in Figs. 3(a)-(c) through a contour plot of the density of (a) component $j = 1$, (b) component $j = 2$, and (c) total density. The stripe soliton and the circularly-asymmetric soliton continue to exist. The resultant densities of the stripe soliton, with a spatial period of π/γ , are illustrated in Figs. 3(d)-(f). The densities of a circularly-asymmetric soliton are depicted in Figs. 3(g)-(i), which are very different from the same

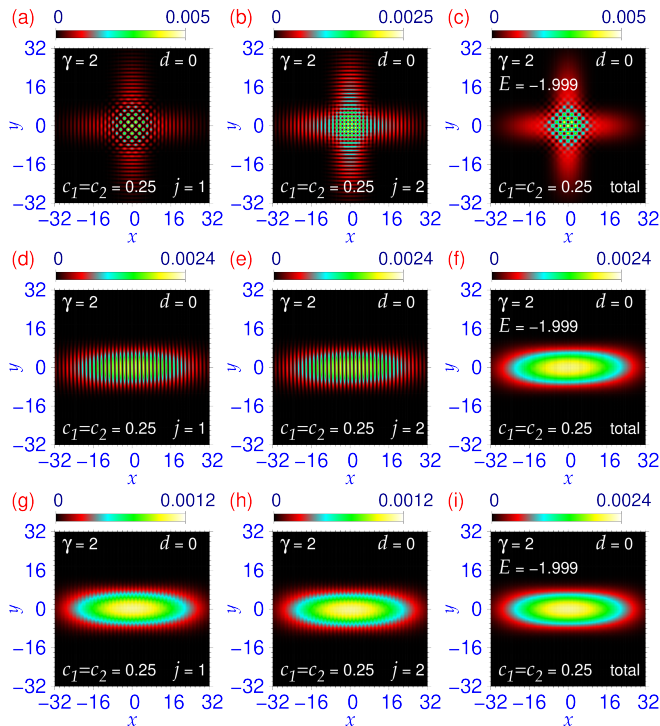


FIG. 3: Contour plot of dimensionless density $n_{2D}(x, y)$ of (a)-(c) a square-lattice soliton, (d)-(f) a stripe soliton, and (g)-(i) a circularly-asymmetric soliton in a self-repulsive nondipolar SO-coupled BEC. The left [middle] column shows the density of component $j = 1(n_1)$ [$j = 2(n_2)$], whereas the right column depicts the total density. The parameters of the model are $c_1 = c_2 = 0.25$ and $\gamma = 2$.

of the circularly-asymmetric soliton of Figs. 1(g)-(i) for $\gamma = 0.5$. Also, there is no prominent vortex-anti-vortex structure in the wave functions of the two components as in the circularly-asymmetric soliton shown in Figs. 1(g)-(h) for $\gamma = 0.5$, viz. Fig. 2(e)-(f). The stripe solitons of Figs. 1(d)-(f) and 3(d)-(f) are quite similar. However, in Figs. 3(a)-(f) the spatially periodic pattern has a small period consistent with $\gamma = 2$. Although, there is a stripe pattern in density for both $\gamma = 0.5$ and $\gamma = 2$, the positions of maxima in component $j = 1$ coincide with the minima in component $j = 2$, thus resulting in a total density without modulation. For $\gamma = 2$, the total density of the stripe soliton in Fig. 3(f) is identical to the same of the circularly-asymmetric soliton in Fig. 3(i), although the component densities are distinct. Hence, for a description of total density and energy, these two binary solitons behave like a unified whole, possessing the same total density and energy. We will see in the following that even in the presence of dipolar interaction the total densities of the stripe soliton and the circularly-asymmetric soliton continue to be equal. In this nondipolar case there is an $x \leftrightarrow y$ symmetry and there is a stripe and a circularly-asymmetric solution aligned along the y axis with the same density and energy as the solitons in Figs. 3(d)-(f) and Figs. 3(g)-(i), respectively (not shown

here). The solitons in Figs. 3(d)-(f) and Figs. 3(g)-(i), although are limited in the identical spatial region, they are distinct. The former has stripes (dark regions) along the y axis; the area of the dark and the bright regions are the same. In the latter, there is no such dark region and the same number of atoms are distributed over the whole area. Consequently, the density in this case is half of the stripe soliton, compare the maximum densities 0.0024 and 0.0012 in the two cases. The numerical energy of the degenerate solitons illustrated in Fig. 3 is $\mathcal{E} = -1.999$ in perfect agreement with the theoretical estimate $\mathcal{E} = -\gamma^2/2$, which for $\gamma = 2$ is $\mathcal{E} = -2$. For a self-attractive nondipolar SO-coupled BEC, we have the same three types of solitons (result not elaborated here).

This spatially-periodic pattern in two and one dimension of the square-lattice and stripe solitons of Figs. 3(a)-(c) and Figs. 3(d)-(f), respectively, is consistent with the periodic supersolid pattern in two [65] and one [75, 76] dimensions. The formation of such supersolid pattern in an SO-coupled spinor BEC has long been demonstrated [74, 77] and studied [78]. The distribution of matter on a square lattice is prominent in Figs. 3(a)-(c), not only in the component densities but also in the total density. The present square-lattice soliton is a consequence of the SO coupling and breaks continuous translational symmetry as required in a supersolid [79–81]. The circularly-asymmetric soliton of Figs. 3(g)-(i) is also distinct.

B. Quasi-2D SO-coupled binary self-repulsive and self-attractive dipolar BEC soliton

The scenario of soliton formation dramatically changes if we consider dipolar atoms with the polarization direction lying along the y axis in the quasi-2D plane. This dipolar interaction is strongly anisotropic in the quasi-2D x - y plane and it will break the circular symmetry of the system. With the introduction of the dipolar interaction, the SO-coupled self-repulsive dipolar system acquires additional attraction and the solitons become more compact and of smaller spatial dimension compared to the nondipolar case considered in Sec. III A. For $\gamma = 0.5$, the multi-ring, stripe and the circularly-asymmetric solitons continue to exist in this case, with much smaller size, as shown in Figs. 4(a)-(l), for $c_1 = c_2 = d = 0.5$. Although, it is possible to have a quasi-2D dipolar soliton with the polarization direction in the quasi-2D plane [45], there is no such soliton for these sets of parameters without an SO-coupling interaction. The dipolar nonlinearity $d = 0.5$ is too weak to support such a soliton. The multi-ring soliton presented in Figs. 4(a)-(c) is of the $(\mp 1, 0)$ type and has the phase structure similar to the same illustrated in Figs. 2(a)-(d) (not explicitly shown in this paper). The stripe soliton presented in Figs. 4(d)-(f) has a spatially periodic stripe along the y axis. As in the nondipolar case, the two components of the spatially asymmetric soliton presented in Figs. 4(g)-(h) host a vortex-anti-vortex structure, which is explicit

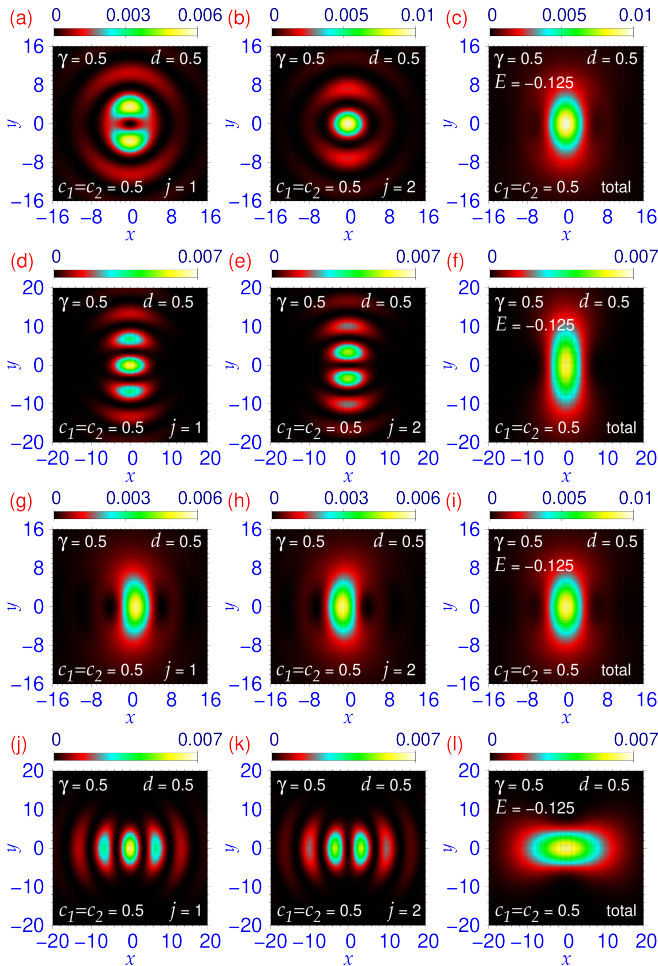


FIG. 4: Contour plot of dimensionless density $n_{2D}(x, y)$ of (a)-(c) a multi-ring soliton, (d)-(f) a stripe soliton with stripes along the y axis, (g)-(i) a circularly-asymmetric soliton, and (j)-(l) a stripe soliton with stripes along the polarization y axis. The left [middle] column shows the density of component $j = 1(n_1)$ [$j = 2(n_2)$], whereas the right column depicts the total density. The parameters of the model are $c_1 = c_2 = d = 0.5$, and $\gamma = 0.5$.

in the plot of the phase of these wave functions in Figs. 2(g)-(h). The total density and energy of the multi-ring soliton presented in Figs. 4(a)-(c) are the same as the circularly-asymmetric soliton illustrated in Figs. 4(g)-(i), although the component densities are distinct. Finally, we find a stripe soliton with stripe along the polarization y axis shown in Figs. 4(j)-(l), which has practically the same density and also the energy as the stripe soliton with stripe along the y axis, indicating an approximate $x \leftrightarrow y$ symmetry for a small $d = 0.5$. All solitons of Fig. 4 are degenerate with energy $\mathcal{E} = -0.125$. We could not find any other type of soliton in this case.

As the SO-coupling strength γ increases beyond $\gamma = 1$, there is some change in the scenario of the formation of a quasi-2D soliton in a binary self-repulsive dipolar BEC, when compared to the same for $\gamma = 0.5$ illustrated in

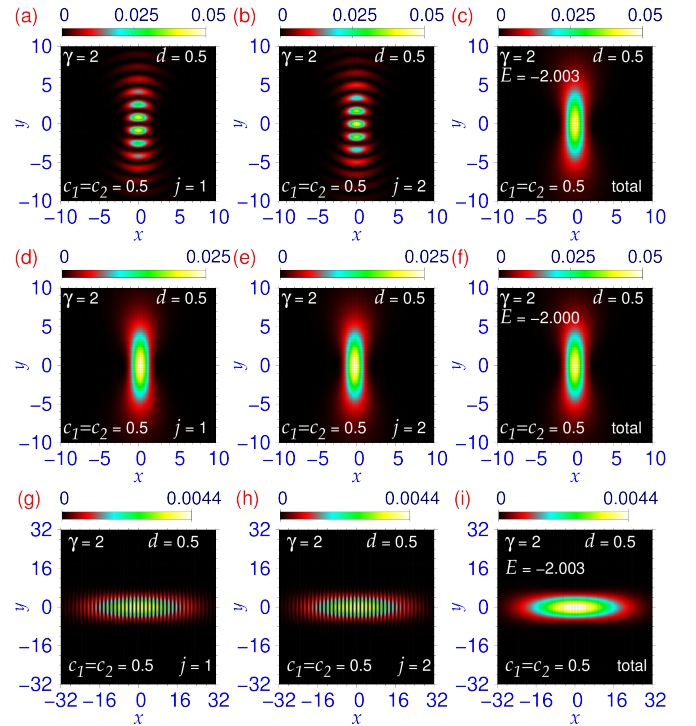


FIG. 5: Contour plot of dimensionless density $n_{2D}(x, y)$ of (a)-(c) a stripe soliton with stripes along the polarization y axis, (d)-(f) a circularly-asymmetric soliton, and (g)-(i) a stripe soliton with stripes along the x axis. The left [middle] column shows the density of component $j = 1(n_1)$ [$j = 2(n_2)$], whereas the right column depicts the total density. The parameters of the model are $c_1 = c_2 = d = 0.5$, $d = 0.5$ and $\gamma = 2$.

Fig. 4. Due to the combined attraction of dipolar interaction and SO coupling, for $\gamma = 2, c_1 = c_2 = d = 0.5$, the multi-ring $(\mp 1, 0)$ -type soliton is squeezed on to the polarization y axis and evolves into a stripe soliton with stripe along the y axes as shown in Figs. 5(a)-(c), obtained in imaginary-time propagation employing a Gaussian initial state imprinted with $(\mp 1, 0)$ angular momenta structure. The converged stripe soliton maintains the approximate $(\mp 1, 0)$ angular momenta structure of the two components. The phase of the wave functions of the two components is presented in Figs. 2(i)-(j). In Fig. 2(i) we find a phase drop of 2π under a complete rotation around the origin corresponding to a an angular momentum projection of $+1$ (vortex of unit angular momentum) in the first component. There is no such vortex in the second component, viz. Fig. 2(j). In addition, for these parameters, we find a circularly-asymmetric soliton as presented in Figs. 5(d)-(f), and a stripe soliton with stripe along the x axes as illustrated in Figs. 5(g)-(i). The circularly-asymmetric soliton possesses a vortex-anti-vortex structure as shown in Fig. 2(k)-(l). The square-lattice soliton is not possible in this case; due to the dipolar attraction along the polarization y axis this soliton is squeezed on the y axis and eventually destroyed.

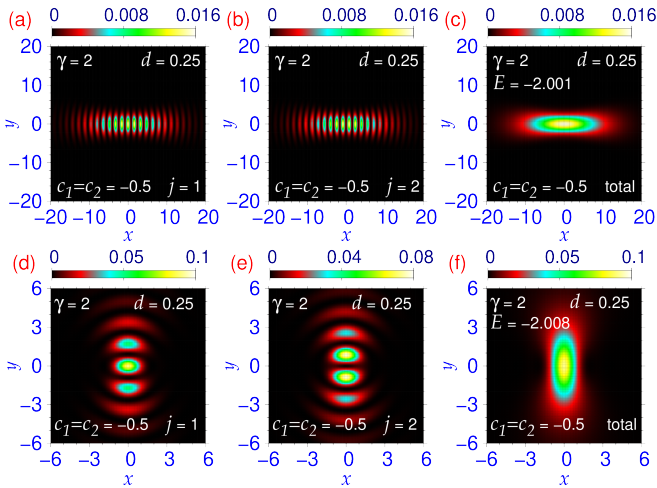


FIG. 6: Contour plot of dimensionless density $n_{2D}(x, y)$ of (a)-(c) a stripe soliton with stripes along the x axis, and (d)-(f) a stripe soliton with stripes along the polarization y axis. The left [middle] column illustrates the density of component $j = 1(n_1)$ [$j = 2(n_2)$], whereas the right column depicts the total density. The parameters of the model are $c_1 = c_2 = -0.5$, $d = 0.25$ and $\gamma = 2$.

The stripe solitons presented in Figs. 5(a)-(c) and Figs. 5(g)-(i), respectively, are degenerate ground states with energy $E = -2.003$, more compact and of smaller size compared to the same solitons in Figs. 4(d)-(f) and in Figs. 4(j)-(l) for $\gamma = 0.5$. The added attraction due to the increased SO-coupling strength is responsible for this. Again, the total density and energy of these two solitons in Figs. 5(a)-(f) are almost identical, although the component densities are distinct, indicating a universal behavior. Of these three solitons presented in Fig. 5 for $\gamma = 2$, the circularly-asymmetric soliton is an excited state with energy ($E = -2.000$). In the presence of strongly anisotropic dipolar interaction in the quasi-2D plane, there is no $x \leftrightarrow y$ symmetry and the stripe soliton aligned along the x axis, viz. Figs. 5(a)-(c), has different density structure from the one aligned along the y axis, viz. Figs. 5(g)-(i).

Although, the principal interest of this paper is the formation of quasi-2D solitons in a self-repulsive SO-coupled dipolar BEC, it is also appropriate to investigate, if any, the changes in the structure of such solitons as the system changes from self-repulsive to self-attractive. To this end, in Fig. 6 we illustrate the densities of the quasi-2D solitons for a self-attractive SO-coupled dipolar BEC for $\gamma = 2$, $c_1 = c_2 = -0.5$, $d = 0.25$. In this case, we reversed the sign of the strengths c_1 and c_2 of the contact interaction and reduced the same of the dipolar interaction d from 0.5 to 0.25. A larger value of d will imply more attraction, which will make the solitons to shrink to have a much smaller size. However, for this set of parameters ($c_1 = c_2 = -0.5$, $d = 0.25$) there is no soliton in the absence of SO coupling; the dipolar nonlinearity ($d = 0.25$) is too small to support a stable soliton. The circularly-

asymmetric soliton of Figs. 5(d)-(f) is not possible in this case due to the added contact attraction. This soliton is eventually destroyed and turns to a stripe soliton with stripe along the y axis. In this case, we find only two types of solitons: a stripe soliton with stripe along the x axis with energy $E = -2.001$ shown in Figs. 6(a)-(c) and a stripe soliton with stripe along the y axis with energy $E = -2.008$ depicted in Figs. 6(d)-(f). Due to an increased contact attraction the solitons of Fig. 6 are more compact and of much smaller size, when compared to the same in Fig. 5. In presence of stronger attraction, away from the linear limit, there is no degeneracy.

IV. SUMMARY AND DISCUSSION

To search for a quasi-2D soliton in a uniform binary SO-coupled dipolar and nondipolar, self-repulsive BEC, using a numerical solution of a mean-field model, we identify a multi-ring soliton, a circularly-asymmetric soliton, a spatially-periodic stripe soliton, and a square-lattice soliton for small to medium strengths of SO coupling γ ($\gamma \lesssim 4$). We consider Rashba and Dresselhaus SO couplings in this paper. In all cases the density obtained with Rashba and Dresselhaus SO couplings are the same although the wave functions and the phases of the solitons are different, viz. Fig. 2. For a small γ ($\gamma \lesssim 1$), there are three types of degenerate states in a nondipolar self-repulsive SO-coupled BEC, viz. Fig. 1: a $(\pm 1, 0)$ -type multi-ring soliton, a circularly-asymmetric soliton, and a stripe soliton. A $(\pm 1, 0)$ -type multi-ring soliton has a vortex or anti-vortex of unit vorticity in one component and no vortex in the other component in addition to having a multi-ring modulation in density of the components without such a modulation in total density, viz. Fig. 1(a)-(c). A stripe soliton has a spatially-periodic stripe in the density of both components and a circularly-asymmetric Gaussian-type total density without stripe, viz., for example, Fig. 1(d)-(f). A circularly-asymmetric soliton of Figs. 1(g)-(i) has a vortex and an anti-vortex in the wave function of each component, viz., Figs. 2(e)-(f). For a medium γ ($1 \lesssim \gamma \lesssim 4$) in a nondipolar self-repulsive SO-coupled BEC we find three types of degenerate solitons, viz. Fig. 3: (a)-(c) a spatially-periodic square-lattice soliton, (d)-(f) a stripe soliton and a (g)-(i) circularly-asymmetric soliton with vortex-anti-vortex structure.

For a dipolar self-repulsive SO-coupled BEC, for a small SO coupling $\gamma = 0.5$, we find four types of degenerate solitons: a multi-ring soliton, a stripe soliton with stripe along the x or y axis, and a circularly-asymmetric soliton, as illustrated in Fig. 4. In the same system, for a large $\gamma (= 2)$, we have three types of solitons: a stripe soliton with stripe along the x or y axis, and a circularly-asymmetric soliton aligned along the y axis, viz. Fig. 5. The stripe solitons with the stripe along the x axis and the polarization y axis are degenerate with the circularly-asymmetric soliton emerging as an excited state. In a

weakly self-attractive dipolar SO-coupled BEC, we find only two types of solitons. e.g. a stripe soliton with stripe along the x axis or the y axis. Of these two type the one with stripe along the x axis is the ground state.

The spatially-periodic density in stripe [74, 75, 77, 78] and square-lattice solitons is a possible manifestation of supersolid-like [79–82] properties. For the small nonlinearities considered in this paper, different types of possible solitons in a self-repulsive SO-coupled nondipolar BEC for a fixed γ are all degenerate with an energy very close to the theoretical estimate $\mathcal{E} = -\gamma^2/2$. For a small γ , the solitonic states in a uniform SO-coupled BEC have a very large spatial extension. For a self-repulsive SO-coupled dipolar BEC, for a small $\gamma = 0.5$ all types of solitons are degenerate; for a medium $\gamma = 2$ this degeneracy is partially broken and the stripe soliton with stripe along the x or y axis are degenerate ground states, whereas the circularly-asymmetric soliton is an excited state. For a medium γ , the total density of the stripe and circularly-asymmetric solitons are found to be almost equal, which seems to be a universal behavior. All these states are dynamically stable, as we verified by real-time simulation over a long period of time (result not presented in this paper). The stripe, square-lattice, and circularly-asymmetric solitons were also found in an SO-coupled nondipolar quasi-2D spin-one [65] and spin-two [98] BECs. However, it is more difficult to perform an experiment in an SO-coupled spin-one or spin-two

BEC with three or five spin components compared to an SO-coupled binary BEC with two spin components. Hence we believe that the present study could motivate experiments in the search of square-lattice states in an SO-coupled binary BEC. The quasi-1D stripe state in a trapped SO-coupled spinor BEC has already been observed and investigated [74]. The square-lattice soliton is dynamically robust and deserve further theoretical and experimental investigation.

ACKNOWLEDGMENT

The author acknowledges support by the Conselho Nacional de Desenvolvimento Científico e Tecnológico (Brazil) grant 303885/2024-6.

DATA AVAILABILITY

The data that support the findings of this article are not publicly available upon publication because it is not technically feasible and/or the cost of preparing, depositing, and hosting the data would be prohibitive within the terms of this research project. The data are available from the authors upon reasonable request.

-
- [1] O. Bang, W. Krolikowski, J. Wyller, and J. J. Rasmussen, *Phys. Rev. E* **66**, 046619 (2002).
- [2] Y. S. Kivshar and B. A. Malomed, *Rev. Mod. Phys.* **61**, 763 (1989).
- [3] F. K. Abdullaev, A. Gammal, A. M. Kamchatnov, and L. Tomio, *Int. J. Mod. Phys. B* **19**, 3415 (2005).
- [4] K. E. Strecker, G. B. Partridge, A. G. Truscott, and R. G. Hulet, *Nature (London)* **417**, 150 (2002).
- [5] L. Khaykovich, F. Schreck, G. Ferrari, T. Bourdel, J. Cubizolles, L. D. Carr, Y. Castin, and C. Salomon, *Science* **256**, 1290 (2002).
- [6] S. L. Cornish, S. T. Thompson, and C. E. Wieman, *Phys. Rev. Lett.* **96**, 170401 (2006).
- [7] V. M. Pérez-García, H. Michinel, and H. Herrero, *Phys. Rev. A* **57**, 3837 (1998).
- [8] E. P. Gross, *Nuovo Cim.* **20**, 454 (1961).
- [9] L.P. Pitaevskii, *Zurn. Eksp. Teor. Fiz.* **40**, 646 (1961)[English Transla.: *Sov. Phys. JETP.* **13**, 451 (1961)].
- [10] L. D. Carr, J. N. Kutz, and W. P. Reinhardt, *Phys. Rev. E* **63**, 066604 (2001).
- [11] O. L. Berman, R. Y. Kezerashvili, G. V. Kolmakov, and L. M. Pomirchi, *Phys. Rev. E* **91**, 062901 (2015).
- [12] L.-C. Zhao, *Phys. Rev. E* **97**, 062201 (2018).
- [13] N.-S. Wan, Y.-E. Li, and J.-K. Xue, *Phys. Rev. E* **99**, 062220 (2019).
- [14] P. Fang and J. Lin, *Phys. Rev. E* **109**, 064219 (2024).
- [15] M. Salerno and B. B. Baizakov, *Phys. Rev. E* **98**, 062220 (2018).
- [16] Y.-H. Qin, L.-C. Zhao, and L. Ling, *Phys. Rev. E* **100**, 022212 (2019).
- [17] S. K. Adhikari, *Phys. Rev. E* **104**, 024207 (2021).
- [18] V. M. Pérez-García and J. B. Beitia, *Phys. Rev. A* **72**, 033620 (2005).
- [19] S. K. Adhikari, *Phys. Lett. A* **346**, 179 (2005).
- [20] R. Y. Chiao, E. Garmire, and C. H. Townes, *Phys. Rev. Lett.* **13**, 479 (1964).
- [21] F. Dalfovo, S. Giorgini, L. P. Pitaevskii, and S. Stringari, *Rev. Mod. Phys.* **71**, 463 (1999).
- [22] J. Stenger, S. Inouye, D. M. Stamper-Kurn, H.-J. Miesner, A. P. Chikkatur, and W. Ketterle, *Nature (London)* **396**, 345 (1998).
- [23] J. Dalibard, F. Gerbier, G. Juzeliunas, and P. Öhberg, *Rev. Mod. Phys.* **83**, 1523 (2011).
- [24] M. H. Anderson, J. R. Ensher, M. R. Matthews, C. E. Wieman, and E. A. Cornell, *Science* **269**, 198 (1995).
- [25] C. C. Bradley, C. A. Sackett, J. J. Tollett, and R. G. Hulet, *Phys. Rev. Lett.* **75**, 1687 (1995).
- [26] K. B. Davis, M. O. Mewes, M. R. Andrews, N. J. van Druten, D. M. Kurn, D. S. Durfee, and W. Ketterle, *Phys. Rev. Lett.* **75**, 3969 (1995).
- [27] V. Galitski and I. B. Spielman, *Nature (London)* **494**, 49 (2013).
- [28] Y. Deng, J. Cheng, H. Jing, C.-P. Sun, and S. Yi, *Phys. Rev. Lett.* **108**, 125301 (2012).
- [29] G. Dresselhaus, *Phys. Rev.* **100**, 580 (1955).
- [30] E. I. Rashba, *Fiz. Tverd. Tela* **2**, 1224 (1960); [English Transla.: *Sov. Phys. Solid State* **2**, 1109 (1960).]
- [31] Y.-J. Lin, K. Jiménez-García, and I. B. Spielman, *Nature*

- (London) 471, 83 (2011).
- [32] J. Li, W. Huang, B. Shteynas, S. Burchesky, F. Ç. Top, E. Su, J. Lee, A. O. Jamison, and W. Ketterle, *Phys. Rev. Lett.* 117, 185301 (2016).
- [33] T. Mizushima, K. Machida, and T. Kita, *Phys. Rev. Lett.* 89, 030401 (2002).
- [34] T. Mizushima, K. Machida, and T. Kita, *Phys. Rev. A* 66, 053610 (2002).
- [35] V. Achilleos, D. J. Frantzeskakis, P. G. Kevrekidis, and D. E. Pelinovsky, *Phys. Rev. Lett.* 110, 264101 (2013).
- [36] H. Sakaguchi, B. Li, and B. A. Malomed, *Phys. Rev. E* 89, 032920 (2014).
- [37] H. Sakaguchi and B. A. Malomed, *Phys. Rev. E* 90, 062922 (2014).
- [38] Y.-C. Zhang, Z.-W. Zhou, B. A. Malomed, and H. Pu, *Phys. Rev. Lett.* 115, 253902 (2015).
- [39] D. Campbell, R. Price, A. Putra, A. Valdés-Curiel, D. Trypogeorgos, and I. B. Spielman, *Nat. Commun.* 7, 10897 (2016).
- [40] S. Gautam and S. K. Adhikari, *Phys. Rev. A* 91, 063617 (2015).
- [41] S. Gautam and S. K. Adhikari, *Phys. Rev. A* 95, 013608 (2017).
- [42] S. Gautam and S. K. Adhikari, *Phys. Rev. A* 97, 013629 (2018).
- [43] S. Inouye, M. R. Andrews, J. Stenger, H.-J. Miesner, D. M. Stamper-Kurn, and W. Ketterle, *Nature (London)* 392, 151 (1998).
- [44] C. Chin, R. Grimm, P. Julienne, and E. Tiesinga, *Rev. Mod. Phys.* 82, 1225 (2010).
- [45] I. Tikhonenkov, B. A. Malomed, and A. Vardi, *Phys. Rev. Lett.* 100, 090406 (2008).
- [46] M. B. Pandey, P. J. Ackerman, A. Burkart, T. Porenta, S. Žumer, and I. I. Smalyukh, *Phys. Rev. E* 91, 012501 (2015).
- [47] M. Johansson, A. A. Sukhorukov, and Y. S. Kivshar, *Phys. Rev. E* 80, 046604 (2009).
- [48] J. Gómez-Gardeñes, B. A. Malomed, L. M. Floría, and A. R. Bishop, *Phys. Rev. E* 74, 036607 (2006).
- [49] Z. Fan, Y. Shi, Y. Liu, W. Pang, Y. Li, and B. A. Malomed, *Phys. Rev. E* 95, 032226 (2017).
- [50] R. M. Wilson, S. Ronen, and J. L. Bohn, *Phys. Rev. A* 80, 023614 (2009).
- [51] L. Santos, G. V. Shlyapnikov, and M. Lewenstein, *Phys. Rev. Lett.* 90, 250403 (2003).
- [52] R. M. Wilson, S. Ronen, H. Pu, and J. L. Bohn, *Phys. Rev. Lett.* 100, 245302 (2008).
- [53] I. Ferrier-Barbut, H. Kadau, M. Schmitt, M. Wenzel, and T. Pfau, *Phys. Rev. Lett.* 116, 215301 (2016).
- [54] M. Guo, F. Böttcher, J. Hertkorn, J.-N. Schmidt, M. Wenzel, H. P. Büchler, T. Langen, and T. Pfau, *Nature (London)* 574, 386 (2019).
- [55] M. A. Norcia, C. Politi, L. Klaus, E. Poli, M. Sohmen, M. J. Mark, R. Bisset, L. Santos, and F. Ferlaino, *Nature (London)* 596, 357 (2021).
- [56] Y. Tang, A. G. Sykes, N. Q. Burdick, J. M. DiSciaccia, D. S. Petrov, and B. L. Lev, *Phys. Rev. Lett.* 117, 155301 (2016).
- [57] T. Lahaye, C. Menotti, L. Santos, M. Lewenstein, and T. Pfau, *Rep. Prog. Phys.* 72, 126401 (2009).
- [58] T. Lahaye, T. Koch, B. Fröhlich, M. Fattori, J. Metz, A. Griesmaier, S. Giovanazzi, and T. Pfau, *Nature (London)* 448, 672 (2007).
- [59] T. Koch, T. Lahaye, J. Metz, B. Fröhlich, A. Griesmaier, and T. Pfau, *Nature Phys.* 4, 218 (2008).
- [60] L. Chomaz, S. Baier, D. Petter, M. J. Mark, F. Wächtler, L. Santos, and F. Ferlaino, *Phys. Rev. X* 6, 041039 (2016).
- [61] K. Aikawa, A. Frisch, M. Mark, S. Baier, A. Rietzler, R. Grimm, and F. Ferlaino, *Phys. Rev. Lett.* 108, 210401 (2012).
- [62] M. Lu, S. H. Youn, and B. L. Lev, *Phys. Rev. Lett.* 104, 063001 (2010).
- [63] S. H. Youn, M. W. Lu, U. Ray, and B. L. Lev, *Phys. Rev. A* 82, 043425 (2010).
- [64] Y. V. Kartashov and D. A. Zezyulin, *Phys. Rev. Lett.* 122, 123201 (2019).
- [65] S. K. Adhikari, *Phys. Rev. A* 103, L011301 (2021).
- [66] M. Kato, X.-F. Zhang, D. Sasaki, and H. Saito, *Phys. Rev. A* 94, 043633 (2016).
- [67] S.-C. Ji, L. Zhang, X.-T. Xu, Z. Wu, Y. Deng, S. Chen, and J.-W. Pan, *Phys. Rev. Lett.* 114, 105301 (2015).
- [68] R. M. Wilson, B. M. Anderson, C. W. Clark, *Phys. Rev. Lett.* 111, 185303 (2013).
- [69] S. Gopalakrishnan, I. Martin, and E. A. Demler, *Phys. Rev. Lett.* 111, 185304 (2013).
- [70] E. Chiquillo, *Phys. Rev. A* 97, 013614 (2018).
- [71] C. Huang, Y. Ye, S. Liu, H. He, W. Pang, B. A. Malomed, and Y. Li, *Phys. Rev. A* 97, 013636 (2018).
- [72] B. Ramachandhran, B. Opanchuk, X.-J. Liu, H. Pu, P. D. Drummond, and H. Hu, *Phys. Rev. A* 85, 023606 (2012).
- [73] S. Autti, V. V. Dmitriev, J. T. Mäkinen, A. A. Soldatov, G. E. Volovik, A. N. Yudin, V. V. Zavjalov, and V. B. Eltsov, *Phys. Rev. Lett.* 117, 255301 (2016).
- [74] J.-R. Li, J. Lee, W. Huang, S. Burchesky, B. Shteynas, F. Ç. Top, A. O. Jamison, and W. Ketterle, *Nature (London)* 543, 91 (2017).
- [75] T. Ozawa and G. Baym, *Phys. Rev. Lett.* 109, 025301 (2012).
- [76] T. Ozawa and G. Baym, *Phys. Rev. Lett.* 110, 085304 (2013).
- [77] A. Putra, F. Salces-Carcoba, Y. Yue, S. Sugawa, and I. B. Spielman, *Phys. Rev. Lett.* 124, 053605 (2020).
- [78] Y. Li, G. I. Martone, L. P. Pitaevskii, and S. Stringari, *Phys. Rev. Lett.* 110, 235302 (2013).
- [79] E.P. Gross, *Phys. Rev.* 106, 161 (1957).
- [80] A. F. Andreev and I. M. Lifshitz, *Zurn. Eksp. Teor. Fiz.* 56, 2057 (1969) [English Transla.: *Sov. Phys. JETP* 29, 1107 (1969)].
- [81] A. J. Leggett, *Phys. Rev. Lett.* 25, 1543 (1970).
- [82] G. V. Chester, *Phys. Rev. A* 2, 256 (1970).
- [83] V. I. Yukalov, *Phys.* 2, 49 (2020).
- [84] D. Mihalache, *Rom. Rep. Phys.* 73, 403 (2021).
- [85] M. Lu, N. Q. Burdick, S. H. Youn, and B. L. Lev, *Phys. Rev. Lett.* 107, 190401 (2011).
- [86] Y. Tang, N. Q. Burdick, K. Baumann, and B. L. Lev, *New J. Phys.* 17, 045006 (2015).
- [87] L. Tanzi, E. Lucioni, F. Famá, J. Catani, A. Fioretti, C. Gabbanini, R. N. Bisset, L. Santos, and G. Modugno, *Phys. Rev. Lett.* 122, 130405 (2019).
- [88] L. Chomaz, I. Ferrier-Barbut, F. Ferlaino, B. Laburthe-Tolra, B. L. Lev, and T. Pfau, *Rep. Prog. Phys.* 86, 026401 (2023).
- [89] Y. Tang, A. Sykes, N. Q. Burdick, J. L. Bohn, and B. L. Lev, *Phys. Rev. A* 92, 022703 (2015).
- [90] C. J. Myatt, E. A. Burt, R. W. Ghrist, E. A. Cornell, and C. E. Wieman, *Phys. Rev. Lett.* 78, 586 (1997).

- [91] D. B. Blasing, J. Pérez-Ríos, Y. Yan, S. Dutta, C.-H. Li, Q. Zhou, and Y. P. Chen, *Phys. Rev. Lett.* 121, 073202 (2018).
- [92] W. Bao and Y. Cai, *Commun. Comput. Phys.* 24, 899 (2018).
- [93] L. Salasnich, A. Parola, and L. Reatto, *Phys. Rev. A* 65, 043614 (2002)
- [94] R. Kishor Kumar, L. E. Young-S., D. Vudragović, A. Balaž, P. Muruganandam, and S. K. Adhikari, *Comput. Phys. Commun.* 195, 117 (2015).
- [95] P. Muruganandam and S. K. Adhikari, *Comput. Phys. Commun.* 180, 1888 (2009)
- [96] V. Lončar, L. E. Young-S., S. Škrbić, P. Muruganandam, S. K. Adhikari, and A. Balaž, *Comput. Phys. Commun.* 209, 190 (2016).
- [97] R. Ravisankar, D. Vudragović, P. Muruganandam, A. Balaž, and S. K. Adhikari, *Comput. Phys. Commun.* 259, 107657 (2021)
- [98] P. Kaur, S. Gautam, and S. K. Adhikari, *Phys. Rev. A* 105, 023303 (2022).